DIRECT NUMERICAL SIMULATION OF A HOMOGENEOUS THERMAL WIND UNDER DENSITY STRATIFICATION

O. Iida and Y. Nagano
Department of Mechanical Engineering,
Nagoya Institute of Technology
Nagoya 466-8555, Japan
iida@heat.mech.nitech.ac.jp

ABSTRACT

In the Earth's atmosphere, zonal currents with a vertical velocity gradient S_u are induced under the action of rotational frequency Ω and horizontal temperature gradient $S_{\theta H}$. These currents satisfying the so-called "thermal wind equation" generate the cyclones and anticyclones through the baroclinic instability, and hence have serious effects on the global circulation. The thermal wind is always under the influence of the density stratification. The effects of density stratification is typically represented by the Richardson number, which is defined as

$$Ri = \left(\frac{N}{S_u}\right)^2, \tag{1}$$

where N and S_u are the buoyancy frequency and the mean shear rate, respectively. At first, we studied the effects of the Richardson number on the thermal wind. With the increase in the Richardson number, the vertical velocity is suppressed and the velocities become two-component. This flow, independent of the Richardson number, becomes vertically collapsed, and the streamwise jets become the dominant flow structure. The pressure gradient becomes almost zero in the streamwise direction, which makes jets homogeneous in this direction.

The critical Richardson number for stabilizing turbulence is strongly dependent on the Coriolis term; the Richardson number needs to increase for stabilizing a shear flow with the large rotational effect. At the sufficiently large Richardson number, however, turbulence becomes vertically collapsed structure as observed in the case of the small Coriolis effect. Interestingly, turbulence cannot be geostrophically balanced between the pressure and the Coriolis terms; the pressure gradient term becomes negligibly small in comparison to the Coriolis term.

INTRODUCTION

Recently, the combined effects of rotation and stratification are attracting the attention from the geophysical point of view (Cambon, 2001 and Rile & Lelong, 2000 are recent review papers on these studies). In almost all these studies, the density stratification is imposed in the gravitational and rotational direction, and hence the baroclinic instability is usually negligible (e.g., Bartello, 1995, Metais et al., 1996, Smith et al., 2002). Although this flow configuration is simple and easy to be numerically simulated, imposing the horizontal temperature gradient is more practical in the geophysical as well as the engineering flows. The horizontal temperature gradient, coupled with the rotation, induces the mean flow, i.e., thermal wind (Gill, 1982).

We numerically simulated the most basic form of the stably stratified thermal wind, i.e., a rotating homogeneous shear flow under density stratification, to study the fundamental effects of rotation, shear and buoyancy on the basic turbulent statistics and structure. Many previous studies indicated that when the strong stable stratification was imposed in a homogeneous shear flow, turbulence collapsed into the horizontally thin layers (e.g., Gerz et al., 1989, Holt et al., 1991 and many others, see Riley & Lelong 2000), although, to authors' knowledge, no study is done for the combined effects of rotation and mean shear.

Stably stratified rotating turbulence, devoid of the internal gravity wave, is represented by either the simplified dynamical equations of Riley et al. (1981) or the stratified quasi-geostrophic equations (Charney, 1971 and many fundamental text books on geostrophic turbulence such as Gill, 1982 and Pedlosky, 1986).

In the quasi-geostrophic equation representing both the low Froude number and the low Rossby number turbulence, the pressure gradient is balanced with the Coriolis terms and the vertically elongated vortex columns become dominant flow structures with the development of the time (McWilliams et al., 1995). When the Froude number is much smaller than the Rossby number, turbulence nondimensionalized by the length scale L and the velocity scale U is represented by the Riley's equation given by:

$$\begin{aligned}&\frac{\partial \mathbf{u_H}}{\partial t} + \mathbf{u_H}\cdot\nabla\mathbf{u_H} + Fr^2 w\frac{\partial}{\partial z}\mathbf{u_H} + \frac{1}{Ro}\mathbf{e_3}\times\mathbf{u_H}\\ =\ & -\nabla_H p + \frac{1}{R_L}\nabla^2\mathbf{u_H},\end{aligned} \tag{2}$$

$$\nabla_H \mathbf{u_H} + Fr^2\frac{\partial w}{\partial z} = 0, \tag{3}$$

$$\begin{aligned}&Fr^2\left(\frac{\partial w}{\partial t} + \mathbf{u_H}\cdot\nabla w + Fr^2 w\frac{\partial w}{\partial z}\right)\\ =\ & -\frac{\partial p}{\partial z} - \rho + \frac{Fr^2}{R_L}\nabla^2 w,\end{aligned} \tag{4}$$

$$\frac{\partial \rho}{\partial t} + \mathbf{u_H}\cdot\nabla\rho + Fr^2 w\frac{\partial \rho}{\partial z} - w = \frac{1}{R_L Pr}\nabla^2\rho, \tag{5}$$

where $Fr(=L/NU)$, $Ro(=L/2\Omega U)$ and $Re(=UL/\nu)$ are the Froude, Rossby and Reynolds numbers, respectively. In the small Froud number limit, the equations are reduced in the following ones,

$$\begin{aligned}&\frac{\partial \mathbf{u_H}}{\partial t} + \mathbf{u_H}\cdot\nabla\mathbf{u_H} + \frac{1}{Ro}\mathbf{e_3}\times\mathbf{u_H}\\ =\ & -\nabla_H p + \frac{1}{R_L}\nabla^2\mathbf{u_H},\end{aligned} \tag{6}$$

$$\nabla_H \mathbf{u_H} = 0, \tag{7}$$

$$0 = -\frac{\partial p}{\partial z} - \rho g, \tag{8}$$

$$\frac{\partial \rho}{\partial t} + \mathbf{u_H} \cdot \nabla \rho - w = \frac{1}{R_L Pr} \nabla^2 \rho. \tag{9}$$

In this Froude number limit, the vertical component of the nondimensionalized velocity becomes negligibly small and the divergence-free condition can be satisfied within the horizontal velocities (see Eq. 7). It also should be noted that the pressure gradient is vertically in balance with the buoyancy (see Eq. 8). As a result, the horizontal velocities are not directly, nor indirectly affected by the buoyancy: both the first and second equations (see Eqs. 6, 7) are solved independently of the other two equations (see Eqs. 8, 9); this equation clearly shows that once turbulence collapses, this structure is independent of buoyancy.

Embid and Majda (1996) decomposed the horizontal velocity field u, satisfying the above equations, into

$$u_H = U_H + \nabla \psi, \tag{10}$$

where $U_H(z,t) = \int u_H(x,y,z,t)dxdy$ is a vertically sheared periodic homogeneous flow (VSHF) and ψ is the horizontal stream function.

The vertical shear U_H satisfies the following equation;

$$\frac{\partial U_H}{\partial t} + \frac{1}{Ro} \times U_H = \frac{1}{Re} \frac{\partial^2}{\partial z^2} U_H. \tag{11}$$

In the above equation, the pressure force does not affect the VSHF. It is also noted that when the vertical shear is horizontally anisotropic, the Coriolis term induces the oscillation between the horizontal velocities as discussed later.

The previous studies (Embid & Majda, 1998; Smith et al., 2002) showed that at large $S(= N/f)$, the non-linear triad interaction enhanced the VSHF fluctuations and attenuated others. However, all these studies are on homogeneous flow without a mean shear and the parameter S is considered to be most important for determining the flow structure. In the stratified shear flow, however, the Richardson number is also considered to determine the flow structure. In our study, a homogeneous shear flow is numerically simulated to study the structure of the thermal wind and discuss which parameter can well represent its turbulent structure.

NUMERICAL METHODS AND FLOW CONDITIONS

Direct numerical simulations of a spectral method are carried out for a homogeneous shear flow under system rotation around the x_3 axis. Both the mean temperature gradient and the gravitational acceleration g are simultaneously imposed in the x_3 direction to include the effects of both buoyancy and rotation. Three-dimensional Navier-Stokes equations are solved numerically. The governing equations for the mean and fluctuation velocities are shown in the following,

-Equations on mean velocity and temperature-

$$\frac{1}{\rho}\frac{\partial P}{\partial x_1} = 0 \tag{12}$$

$$\frac{1}{\rho}\frac{\partial P}{\partial x_2} = -2\Omega U_1 \tag{13}$$

$$\frac{1}{\rho}\frac{\partial P}{\partial x_3} = g\beta\Theta \tag{14}$$

-Equations on velocity and temperature fluctuations-

Table 1: Flow conditions at $S_u/\Omega = 20$

	TW0.1A	0.2A	0.3A	0.5A	1A	36A
Ri	0.1	0.2	0.3	0.5	1	36
Pr				0.71		
S	3.16	4.47	5.48	7.07	10	60
C_θ	-1	-0.5	-0.333	-0.2	-0.1	-2.78×10^{-3}
Re_0				65.4		
S^*_0				0.798		
Ro_0				12.5		
Fr_0	3.96	2.80	2.29	1.77	1.25	0.209

The subscript 0 represents the initial value.

Table 2: Flow conditions at $S_u/\Omega = 1$

	0.25B	0.5B	0.8B	1B	2B	8B	16B	36B
Ri	0.25	0.5	0.8	1	2	8	16	36
Pr					0.71			
S	0.25	0.354	0.447	0.5	0.707	1.41	2	3
C_θ	-8	-4	-2.5	-2	-1	-0.25	-0.125	-0.056
Re_0					65.4			
S^*_0					0.798			
Ro_0					0.626			
Fr_0	1.25	1.77	1.40	1.25	0.885	0.442	0.313	0.209

Table 3: Flow conditions of $S_u/\Omega \neq 1$, 20

Case	TW0.5C	0.5D	0.5E	1C	1D	1E	1F
Ri		0.5				1	
Pr				0.71			
S	0.014	0.088	0.177	0.02	0.125	0.25	2.5
S_u/Ω	0.04	0.25	0.5	0.04	0.25	0.5	5
C_θ	-100	-16	-8	-50	-8	-4	-0.4
Re_0				65.4			
S^*_0	0.159	0.399	0.798	0.160	0.399	0.798	3.99
Ro_0	0.125	0.313	0.313	0.125	0.313	0.313	0.626
Fr_0	8.86	3.54	1.77	6.26	2.50	1.25	0.25

$$\frac{\partial u_i}{\partial t} + u_j \frac{\partial u_i}{\partial x_j} = -U_1 \frac{\partial u_i}{\partial x_1} - u_3 S_u \delta_{i1} - \frac{1}{\rho}\frac{\partial p}{\partial x_i} + \nu \frac{\partial^2 u_i}{\partial x_j \partial x_j} - 2\Omega(-u_2\delta_{i1} + u_1\delta_{i2}) + g\beta\theta\delta_{i3} \tag{15}$$

$$\frac{\partial u_i}{\partial x_i} = 0 \tag{16}$$

$$\frac{\partial \theta}{\partial t} + u_j \frac{\partial \theta}{\partial x_j} = -U_1 \frac{\partial \theta}{\partial x_1} - u_2 S_{\theta H} - u_3 S_{\theta V} + \alpha \frac{\partial^2 \theta}{\partial x_j \partial x_j} \tag{17}$$

In the above equations, capital letters represent the mean values, while small letters represent fluctuations. Mean velocity gradient is represented by S_u, while $S_{\theta H}$ and $S_{\theta V}$ represent mean horizontal and vertical temperature gradient, respectively. In the thermal wind, the following relation between shear and temperature gradient will be obtained by taking the curl of Eqs. 13 and 14,

$$S_{\theta H} = -2\Omega S_u / g\beta. \tag{18}$$

In the flow with a mean shear induced by the baroclinic instability, the flow stability should be considered, which is possibly determined by the Richardson number. In the earth's atmosphere, Ri is approximately about 100 when the mean shear is relatively weak in comparison to buoyancy (McIntyre, 2000). On the other hand, $S(= N/f)$ is about 10 in the ocean and 100 in the atmosphere(Gill, 1977). Hence, S_u/Ω is about 10 in the atmosphere when the mean shear is relatively weak. In our numerical simulation, both cases of S_u/Ω=1, 20 are studied at the different Richardson numbers, to clarify the rotational effect.

The flow conditions of these cases are listed in Tables 1, 2 and 3. In the cases of S_u/Ω=20, which are represented by

the case of A, the Richardson number is varied from 0.1 to 36. In these cases, N/f is much larger than 1 and approximately the same value as the ocean and the atmosphere. On the other hand, in the cases of S_u/Ω=1 represented as B, the Richardson number is from 1 to 36, and N/f is almost equal to or less than 1.

RESULTS AND DISCUSSIONS

At first, we will discuss the instability of flow at the different Richardson numbers and the different S_u/Ω. Secondly, the structure of collapsed turbulence at the large Richardson number and its dependence on the Coriolis term is studied.

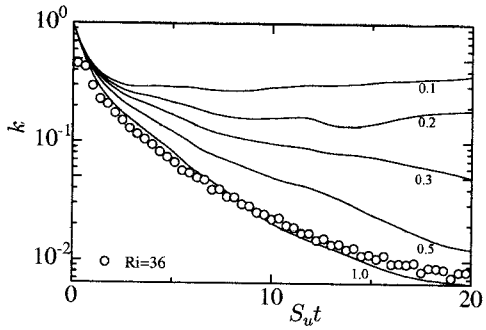

Figure 1: Time development of turbulent kinetic energy at different Richardson numbers in cases of $S_u/\Omega = 20$.

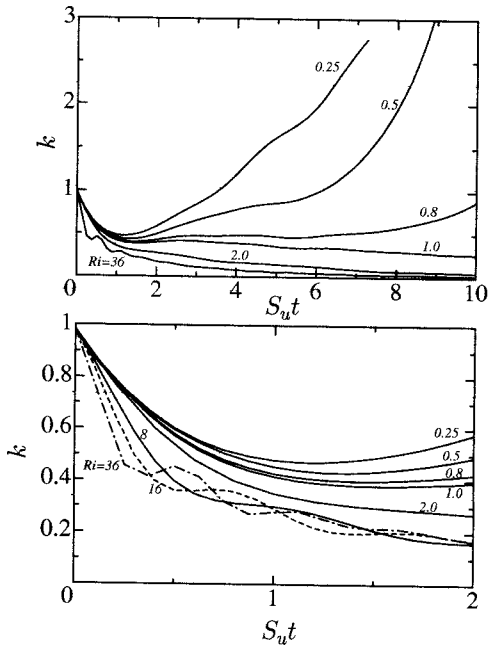

Figure 2: Time development of turbulent kinetic energy at different Richardson numbers in cases of $S_u/\Omega = 1$.

Figs. 1 and 2 show the time development of the turbulent kinetic energy in the cases of the different Richardson numbers. In the stably stratified shear flow, the critical Richardson number, i.e., the criteria for the flow stability, is approximately 0.25. In the cases of $S_u/\Omega = 20$, the critical Richardson number is almost 0.3 and in agreement with the previous criteria (see Fig. 1). This condition, however, cannot be applied to the thermal wind, which definitely unstable at this Richardson number. In this flow condition, the density stratification needs to further increase for attenuating the flow instability. In the flow of $Ri > 1$, however, turbulent kinetic energy decays with the development of the time and the critical Richardson number should be around this.

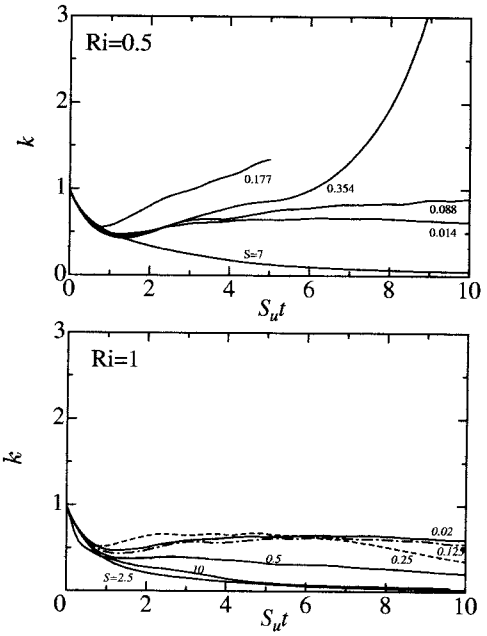

Figure 3: Time development of turbulent kinetic energy at two different Richardson numbers of several different $S = N/2\Omega$.

We study how $S(= N/f)$ affects the flow instability at Ri =0.5 and 1, where turbulence decays and increases, respectively (see Fig. 3). In any cases of the Richardson number, the smaller S, i.e., large rotational effect, reduces the correlation among the velocity and the temperature fluctuation, which attenuates the buoyancy effect as well as the shear instability. Hence, increase in turbulence kinetic energy is leveled off and turbulence reaches the equilibrium state.

This rotational effect, however, depends on the Richardson numbers. At $Ri < 1$, the large N/f enhances the flow instability and increases the turbulence kinetic energy, although the further increase in N/f stabilizes the flow. On the other hand, at $Ri \geq 1$, the increase in N/f attenuates the flow instability and reduces the turbulence energy; this flow condition is almost always satisfied in the environmental flow.

In the next, we study the Richardson number effects on the turbulent structure. Figure 4 shows the time development of the second and the third invariants on the Reynolds stresses, which are plotted on the Lumley's invariant map (Lumley & Newman, 1977). At the smaller Ri, the plot approaches upward to the right-hand-side of the triangle, which represents turbulence having one larger component of the Reynolds stresses than the others; the shear instability enhances the streamwise component of the Reynolds stresses. At the large Ri, however, the plot approaches to the upper-side of the triangle and turbulence becomes two-component as typically observed in stratified turbulence.

To investigate the further detail of the flow structure, we study the time development of the Reynolds normal stresses in the cases of the different Richardson numbers and the different S_u/Ω (Figs. 5 and 6). In the case of $S_u/\Omega = 20$,

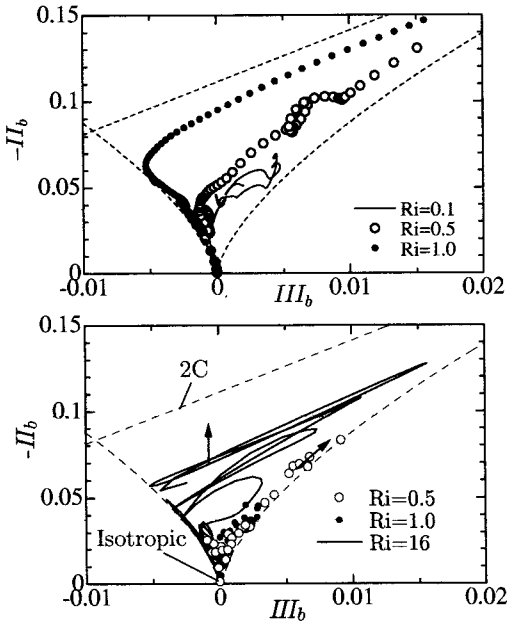

Figure 4: Time development of second and third invariants of Reynolds stresses.

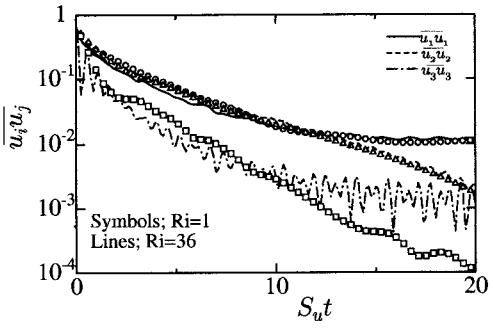

Figure 5: Time development of Reynolds normal stresses at Ri=1, 36 of $S_u/\Omega = 20$.

it is noted that each horizontal Reynolds stress at the large Richardson numbers is collapsed into the single curve. This is also true in the cases of $S_u/\Omega = 1$; no definite difference observed in the cases of Ri =4, 8, 16, 36 indicates that the turbulent structure is independent of the Richardson number after the turbulence collapse. This should be because collapsed turbulence is dynamically governed by the Liley's equation where the velocity equations are independent of buoyancy.

There is a notable difference between $S_u/\Omega = 1$ and 20; in the case of $S_u/\Omega = 1$, $\overline{u_1^2}$ and $\overline{u_2^2}$ oscillate and exchange their energy. Their oscillation frequency is the half of Ω, though each fluctuating velocity oscillates at Ω.

The time development of the velocity spectra is shown in Figs. 7 and 8. We can see that with the development of the time, the energy of the streamwise velocity is concentrated in the region of $k_1 = 0$; the flow becomes homogeneous in the streamwise directions. In the spanwise direction, the most energy is concentrated in both $k_3 = 0$ and 1 regions. The energy in the other regions of the wavenumbers is almost negligible, indicating that the collapsed turbulence is almost VSHF and governed by Eq. 11.

The instantaneous isosurfaces of the streamwise and the

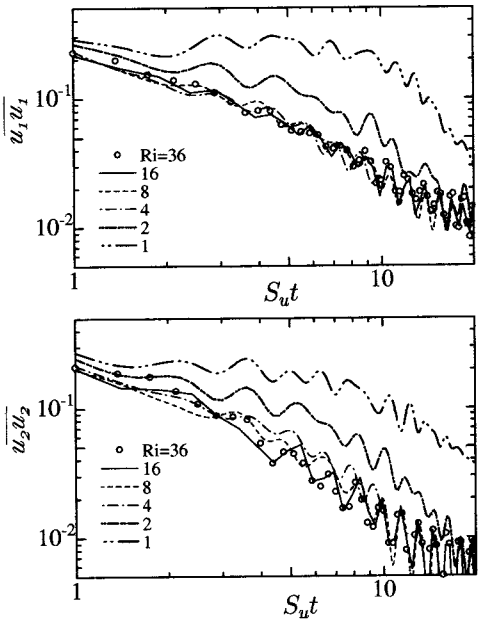

Figure 6: Time development of Reynolds normal stresses at Ri=1 to 36 of $S_u/\Omega = 1$.

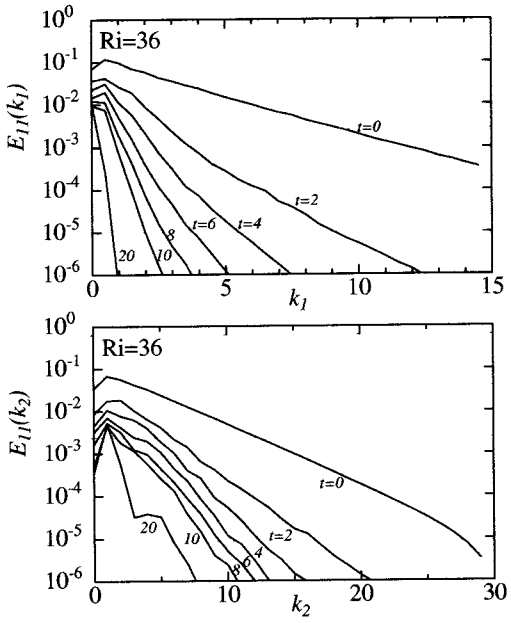

Figure 7: Time development of energy spectra $E_{11}(k_1)$ and $E_{11}(k_2)$ from $t = 0$ to 20 in the case of S_u/Ω=20 and Ri=36.

spanwise velocities are shown in Figure 9. All isosurfaces in the figures are extended into the streamwise direction and representing the jet structures. It is also noted that the jets of the different directions are piled up on each other.

For further detail, the typical example of the instantaneous velocity vectors is shown in Figs. 10. The two streamwise jets of the opposite flow direction are clearly noted; the velocity vectors are mostly aligned in the streamwise direction. The pressure fluctuation takes longitudinally constant, which makes the flow homogeneous in this direction. On the other hand, there is the spanwise pressure gradient which redirects the spanwise velocity into the ver-

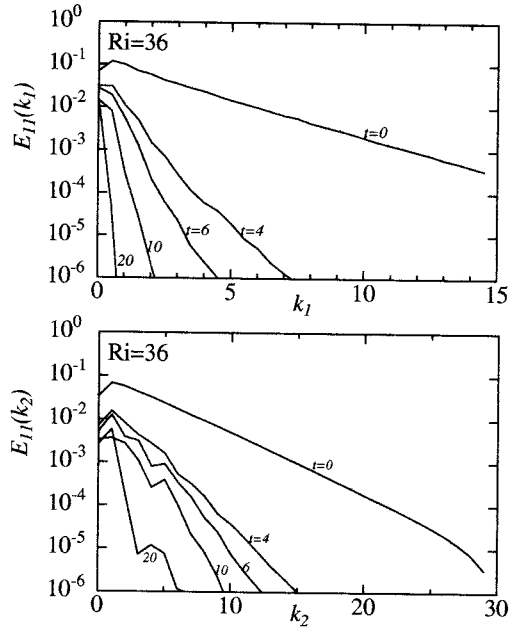

Figure 8: Time development of energy spectra $E_{11}(k_1)$ and $E_{11}(k_2)$ from $t = 0$ to 20 in the case of S_u/Ω=1 and Ri=36.

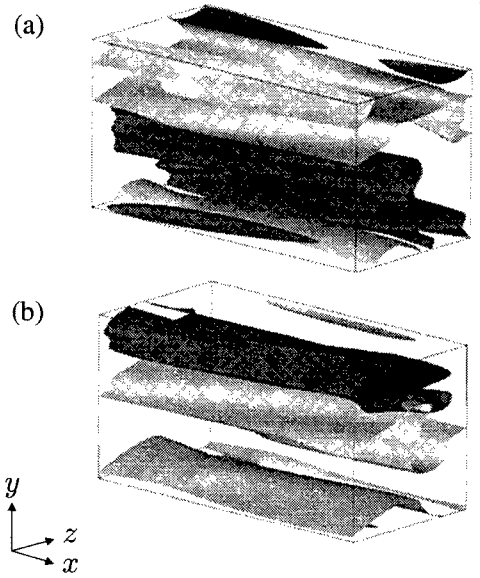

Figure 9: Isosurfaces of horizontal velocities u and v in case of $Ri = 36$ and $S_u/\Omega = 20$, (a) Black, $u = -1.5$; Gray, $v = 0.5$, (b) Black, $u = 1.5$; Gray, $v = -0.5$.

tical one and makes it smaller than the streamwise one as shown in Fig. 5. The above-mentioned jet structure as well as collapsed turbulence is observed also in the case of strong rotation effect, though not shown here.

Finally, the transport mechanism of the Reynolds stresses is studied in collapsed turbulence. Figures 11 and 12 show the budget of $\overline{u^2}$ and $\overline{v^2}$ in the cases of S_u/Ω=1 and 20. In the case of S_u/Ω=20, the production term of $\overline{u_1^2}$ is balanced by the time derivative term, while both the Coriolis term and the streamwise pressure-strain term are negligibly small after $t = 4$. In the $\overline{v^2}$ budget, the pressures-strain term

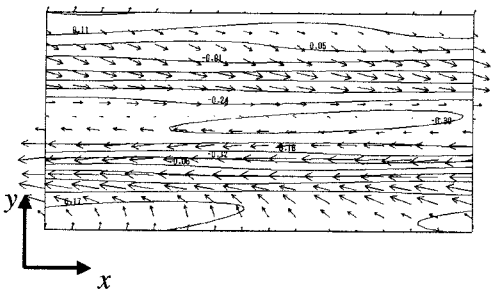

Figure 10: Velocity vectors in x-y plane and contours of pressure fluctuations, St=20, $S_u/\Omega = 20$, $Ri = 36$.

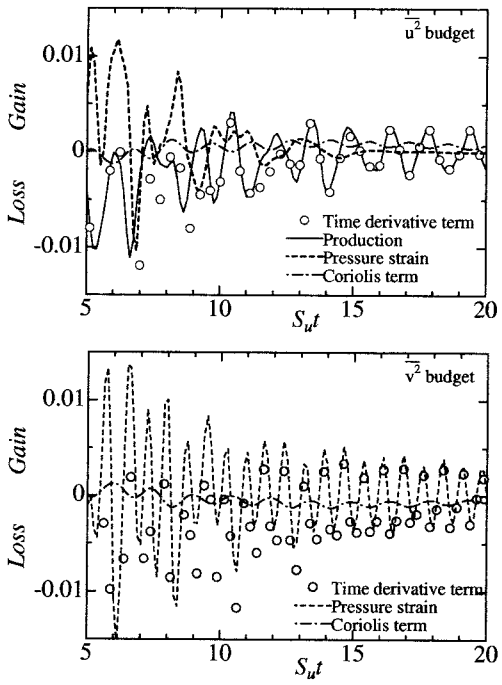

Figure 11: Budget of $\overline{u_1^2}$ and $\overline{u_2^2}$ at $Ri = 36$ of $S_u/\Omega = 20$.

is balanced by the time derivative term. Figure 11 indicates that this flow is governed by the equation associated with the VSHF in the streamwise direction and the pressure term is negligible in this direction.

At S_u/Ω=1 (see Fig. 12), the time derivative term is balanced by the Coriolis term; both the production term and the pressure-strain term are negligibly small in comparison to the Coriolis term. This is also true in $\overline{v^2}$, and the pressure-strain term is almost negligible in comparison to the others. This flow is also governed by the VSHF equation and the Coriolis terms is balanced by the time derivative terms in both horizontal and streamwise directions.

CONCLUSION

In the thermal wind, even if the Coriolis term is included, the Richardson number still becomes the most important parameter to determine the flow structure. As long as the Richardson number is sufficiently large, turbulence becomes

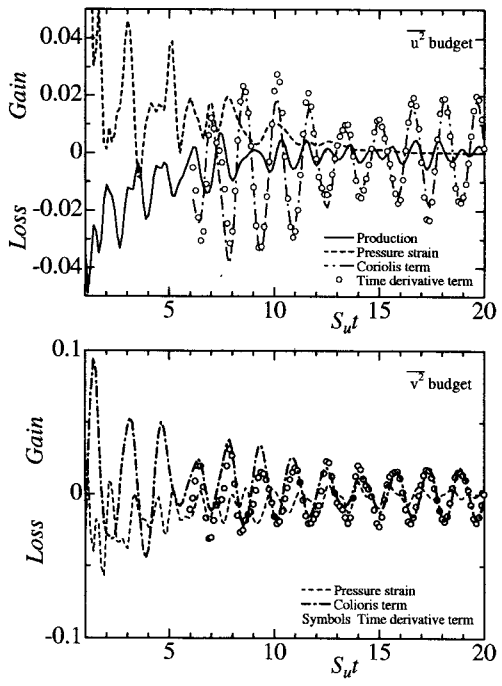

Figure 12: Budget of $\overline{u_1^2}$ and $\overline{u_2^2}$ at $Ri = 36$ of $S_u/\Omega = 1$.

two-component: the horizontal components of the Reynolds stresses surpass the vertical component. Once turbulence collapses, however, the Richardson number does not affect turbulent structure because the horizontal velocities become independent of the buoyancy.

After turbulence collapses, the flow becomes homogeneous in the streamwise direction and the streamwise jets become the dominant flow structures. This flow structure is mostly governed by the VSHF equations used for strongly stratified flow, where the pressure gradient term becomes almost negligible in the horizontal direction.

The critical Richardson number Ri_c for turbulence collapse depends on the rotational effects. At the large S_u/Ω, Ri_c is almost the same as the typical value used in stratified turbulence. At the small S_u/Ω, however, the flow is more unstable, and the Richardson number must be increased to level off the turbulent kinetic energy.

In the budget equations of the horizontal Reynolds stresses, the pressure-strain term becomes negligibly small in comparison to the Coriolis term or the production term. Especially at the large rotational effect, the Coriolis term dominates the budget equations of the horizontal Reynolds stresses and the time derivative terms are, as a result, balanced by the Coriolis term, which results in the oscillation of the horizontal velocities.

ACKNOWLEDGEMENT

This work was supported by the Ministry of Education, Science, Sports and Culture through Grant-in-Aid for Scientific Research (B) (No. 10450085).

REFERENCES

C. Cambon, "Turbulence and vortex structure in rotating and stratified flows," Eur. J. Mech. B-Fluids **20**, 489 (2001).

J. J. Riley and M. P. Lelong, "Fluid motions in the presence of strong stable stratification," Ann. Rev. Fluid Mech. **32**, 613 (2000).

P. Bartello, "Geostrophic adjustment and inverse cascade in rotating flows," J. Atmos. Sci., **52**, 4410 (1995).

O. Metais, P. Bartello, E. Garnier, J. J. Riley and M. Lesieur, "Inverse cascade in stably stratified rotating turbulence," Dynamics of Atmospheres and Oceans **23**, 193 (1996).

L. M. Smith and F. Waleffe, "Generation of Slow, Large Scales in Forced Rotaing, Stratified Turbulence," J. Fluid Mech. (2001).

A. E. Gill, *Atmosphere-Ocean Dynamics* (Academic Press, New York, 1982).

T. Gerz, U. Schumann, S. E. Elghobashi, Direct numerical simulation of stratified homogeneous turbulent shear flows, J. Fluid Mech. **200** 563 (1989).

S. E. Holt, J. R. Koseff, J. H. Ferziger, A numerical study of the evolution and structure of homogeneous stably stratified turbulence, J. Fluid Mech. **237** 499 (1992).

J. Riley, R. Metcalfe and M. Weissman, "Direct numerical simulations of homogeneous turbulence in density stratified fluids," *Proc. AIP Conf., No. 76, Nonlinear Properties of Internal Waves*, Ed., B. J. West, pp. 79-112, 1981.

J. G. Charney, "Geostrophic turbulence ," J. Atmos. Sci. **28**, 1087 (1971).

J. Pedlosky, *Geophysical Fluid Dynamics* (Springer, New York, 1986).

J. C. McWilliams, J. B. Weiss and I. Yavneh, "Anisotropy and coherent vortex structures in planetary turbulence," Science **264**, 410 (1994).

P. F. Embid and A. J. Majda, "Low Froud number limiting dynamics for stably stratified flow with small or finite Rossby number," Geophys. Astrophys. Fluid Dynamics, **87**, 1(1998).

M. E. McIntyre, "On global-scale atmospheric circulation," (In Perspectives in Fluids Dynamica, edited by G. K. Batchelor et al, Cambridge Univ. Press, Cambridge, UK, 2000), p.574.

J. Lumley and G. Newman, "The return to isotropy of homogeneous turbulence," J. Fluid Mech. **82**, 161 (1977).